

CLASSIFICATION OF PULSARS USING EXTREME DECONVOLUTION

TARUN TEJ REDDY CH.

Department of Electrical Engineering, IIT Hyderabad, Kandi, Telangana 502285, India
ee17btech11042@iith.ac.in

SHANTANU DESAI

Department of Physics, Indian Institute of Technology Hyderabad, Kandi, Telangana 502285, India
shntn05@gmail.com

Submitted to The Open Journal of Astrophysics

ABSTRACT

We carry out a classification of all the observed pulsar population into distinct clusters, based on their period and period derivatives, using Extreme Deconvolution based Gaussian Mixture Model. We then use the Bayesian Information criterion to select the optimum number of clusters. We find in accord with previous works, that the pulsar dataset can be optimally classified into six clusters, with two for the millisecond pulsar population, and four for the normal pulsar population. Using numerical experiments, we confirm that Extreme Deconvolution-based classification is not sensitive to variations in the dataset. All our analysis codes used for this work have been made publicly available.

Subject headings: radio pulsars: classification Extreme Deconvolution

1. INTRODUCTION

Pulsars are rotating neutron stars with pulsed radio emission, attributed to a rotating magnetic dipole. Ever since their first serendipitous discovery (Hewish et al. 1968), a whole zoo of neutron stars with considerable diversity have been discovered throughout the electromagnetic spectrum. However, the most common manifestation of neutron stars are usually pulsars detected in radio waves. Pulsars have proved to be wonderful laboratories for a whole bunch of topics in Physics and Astronomy, such as exoplanets, gravitational waves, study of nuclear matter at high densities, dark matter, stellar evolution, probes of interstellar medium, etc (Blandford 1992; Lorimer & Kramer 2012; Kaspi & Kramer 2016; Desai & Kahya 2016; Manchester 2017).

The two main observables which typically characterize a radio pulsar are its period (P) and period derivatives (\dot{P}). From these, one can derive estimates of their ages and magnetic fields. Radio pulsars can be broadly classified into two types. The first category is classical radio pulsars with $P > 0.2$ seconds, \dot{P} between 10^{-16} and 10^{-13} seconds, magnetic fields between $10^{10} - 10^{13}$ G. These pulsars are usually associated with supernova remnants. The second category is millisecond pulsars, with periods less than 0.2 seconds and $B < 10^9$ G. The origin of these pulsars is different from the classical radio pulsar population, and these are believed to be the descendants of low-mass X-ray binaries (Bhattacharya & van den Heuvel 1991). More than 250 millisecond pulsars have also been discovered in gamma rays by the Fermi-LAT satellite, some of which are new discoveries, and have not yet been detected in the radio (Acero et al. 2015). As of now, the total number of known pulsars is close to 3,000 and we expect to discover about 20,000 new pulsars in the SKA era (Kramer & Stappers 2015).

Subsequently, a whole zoo of neutron stars with diverse characteristics have since been discovered such as magnetars, rotating radio transients, X-ray dim isolated

neutron stars, Fast Radio bursts, Central compact objects etc (Woods & Thompson 2006; Kaspi 2010; Safi-Harb 2017; Harding 2013; De Luca 2017; Konar 2017; Enoto et al. 2019; Cordes & Chatterjee 2019). Because of the proliferation of distinct observational classes of neutron stars, a number of automated techniques have been used to classify the pulsar population into disparate classes, as well as to understand the connection between them. The first class of techniques involve the study of evolutionary tracks along the $P-\dot{P}$ diagram, also called “pulsar current” analysis (Vivekanand & Narayan 1981; Vranešević & Melrose 2011; Glushak 2020). The second group of efforts involves the application of unsupervised clustering techniques. The first work along these lines was carried out by Lee et al. (2012), who applied the Gaussian mixture model (GMM, hereafter) in the $P-\dot{P}$ plane to radio pulsars from the ATNF catalog (Manchester et al. 2005), as well as gamma-ray pulsars from the Fermi-LAT 2 year point source catalog (Nolan et al. 2012). They found a total of six clusters (two for the millisecond pulsar population and four for the normal pulsars). However, Igoshev & Popov (2013) pointed out that for rapidly evolving objects, GMM is oversensitive to the pulsar dataset and does not produce stable results. Ay et al. (2020) then used Dirichlet process GMM to classify radio pulsars from the ATNF catalog in conjunction with other types of neutron star such as SGRs, AXPs, RRATs, CCOs, and XDINS. Their analysis also confirms the presence of two clusters for the millisecond pulsar population and four for the rest.

In this work, for the purpose of pulsar classification, we incorporate the errors in the observed P and \dot{P} , and use an extension of GMM, known as Extreme Deconvolution. The outline of this paper is as follows. A brief discussion of Extreme Deconvolution based GMM is given in Sect. 2. Details of our analysis and results can be found in Sect. 3. We conclude in Sect. 4. All our codes used for this analysis have been made publicly available, for

which the relevant link can be found in Sect. 4.

2. EXTREME DECONVOLUTION

The problem of density estimation and finding clusters in a given dataset has widespread applications throughout Astrophysics. For this purpose, a large number of techniques involving unsupervised clustering have been applied to a variety of problems (Ball & Brunner 2010; Ivezić et al. 2014; Fraix-Burnet et al. 2015; Fluke & Jacobs 2020).

A large class of these clustering algorithms involving Parametric density estimation come under the guise of “Mixture models” (Ivezić et al. 2014; Kuhn & Feigelson 2017). The most widely used mixture models use Gaussian components, and hence is called GMM. Although mixture models with non-Gaussian distributions have also been used in astrophysical literature (Tarnopolski 2019), the central limit theorem assures us that the assumption of Gaussianity within each cluster is a reasonable one for any mixture model. In traditional GMM, data is modelled by fitting it with a weighted sum of multiple Gaussian distributions, with each component having separate means and covariance. GMM has been widely for a plethora of classification problems in astrophysics (Kuhn & Feigelson 2017).

Inferring distributions of the data which involve uncertainties (which is ubiquitous in Physics and Astronomy) is even more challenging, as the noise for each observation could be generated due to an unknown source and the error distribution is not always known. This extension of GMM which incorporates the errors the data in known in the Astrophysics literature as Extreme Deconvolution (XDGM) (Bovy et al. 2011; Ivezić et al. 2014; Holoien et al. 2017). We first provide a brief mathematical preview of GMM, and then outline how it can be generalized to XDGM by including the errors. More details on XDGM are provided in the above works.

The traditional GMM models the distribution as a mixture of Gaussian clusters. Each Gaussian cluster has a weight, a central data point (mean) and variance associated with it. The likelihood of each data point (x) for a GMM is given by:

$$p(x) = \sum_{j=1}^K \alpha_j \mathcal{N}(x | \mu_j, \Sigma_j), \quad (1)$$

where, α_j , μ_j and Σ_j are the weights, means, and variances of the j^{th} Gaussian cluster, $\mathcal{N}(x | \mu_j, \Sigma_j)$ is the Gaussian probability density function of the j^{th} gaussian cluster, K is the total number of clusters. The sum of all the weights (α_j) is equal to one. The best-fit parameters for each of the clusters are found using Expectation-Maximization (EM) algorithm Roche (2011).

XDGM now generalizes the traditional GMM, by taking into account the uncertainty distribution of each data point, while calculating the likelihood of the model for each data point. We assume that the noisy dataset x_i is related to the true values v_i as follows (Bovy et al. 2011; Ivezić et al. 2014):

$$x_i = R_i v_i + \epsilon_i, \quad (2)$$

where R_i is the projection matrix. The noise ϵ_i is assumed to be drawn from a Gaussian with zero mean and

variance S_i . Then, the likelihood of the model parameters ($\theta = \alpha, \mu, \Sigma$) for each data point is given as,

$$p(x_i | \theta) = \sum_{j=1}^K \alpha_j \mathcal{N}(x_i | R_i \mu_j, R_i \Sigma_j R_i^T + S_i) \quad (3)$$

The final step is to find the objective function to determine the free parameters of the model. This can be done (as in GMM) by summing up the individual log-likelihood functions.

$$\phi = \sum_{i=1}^N \ln(p(x_i | \theta)), \quad (4)$$

where N is the total number of datapoints. Similar to GMM, a simple extension of the EM algorithm (discussed in Bovy et al. (2011)) is used to maximize the objective function in XDGM. The EM algorithm iteratively maximizes the likelihood, and hence results in the optimal values of the model parameters.

XDGM has proven to be useful in modelling the underlying distributions, where the data points have noise associated with them, such as the velocity distribution from Hipparcos data (Bovy et al. 2011), the three-dimensional motions of the stars in Sagittarius streams (Koposov et al. 2013), classification of neutron star masses (Keitel 2019), identification of dark matter subhalo candidates (Coronado-Blázquez et al. 2019) etc.

3. ANALYSIS AND RESULTS

We now apply the XDGM algorithm to classify the pulsar population in the P - \dot{P} plane. First, we describe the dataset used for the analysis, followed by the implementation of the XDGM algorithm. We then discuss the metric used for choosing the optimum number of Gaussian components, and finally present our results.

3.1. Data Collection

For this work, we downloaded P and \dot{P} for the radio pulsar population, along with the measurement errors from the ATNF online catalogue (version 1.64) (Manchester et al. 2005)¹. The ATNF catalog contains an up-to-date list of all the discovered pulsars. At the time of writing, there were exactly 2,289 pulsars with known errors in P and \dot{P} and positive values for \dot{P} . This catalog also contains 522 pulsars with either negative values for \dot{P} or missing errors for P or \dot{P} . These 522 pulsars were excluded from our analysis.

The distribution of P and \dot{P} for these 2289 pulsars is shown in Fig. 1. Unlike Lee et al. 2012; Ay et al. 2020, we did not include ancillary neutron stars such as RRATs, CCO, gamma-ray pulsars (from Fermi-LAT), since the error estimates for P and \dot{P} for these datasets were not available. However, it is trivial to include these in our analysis, if their error estimates are made available.

3.2. XDGM for Pulsar Classification

We now apply XDGM to the pulsar dataset. Since both the P and \dot{P} values have a large dynamic range

¹ <http://www.atnf.csiro.au/research/pulsar/psrcat/>

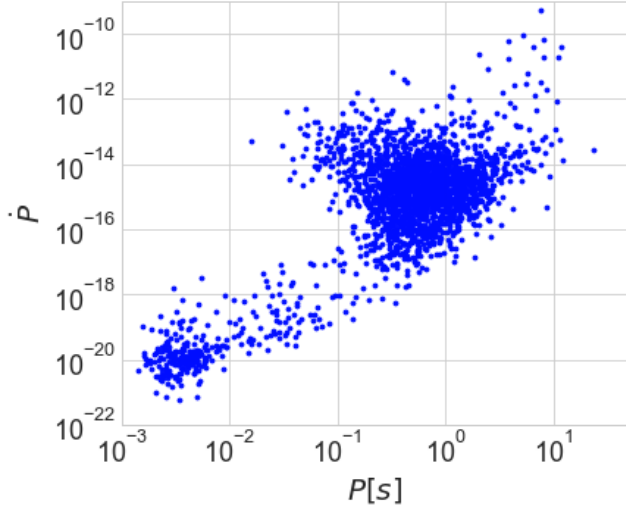


FIG. 1.— Pulsar P - \dot{P} diagram using the online ATNF catalog (Manchester et al. 2005).

spanning many orders of magnitude, the inputs given to the XDGMM algorithm are $\ln(P)$ and $\ln(\dot{P})$, similar to Lee et al. (2012); Ay et al. (2020). The errors in these transformed variables are obtained by error propagation.

For this work, we used the implementation of XDGMM from the `astroML` python module (Ivezić et al. 2014). The dataset provided as input to the XDGMM code consists of $\ln(P)$ and $\ln(\dot{P})$. Since, we need to classify the pulsars using a 2-d dataset, we vertically stack the $\ln(P)$ and $\ln(\dot{P})$ values, and provide the resulting matrix as input to the XDGMM algorithm. Therefore, we get two error covariance matrices for every 2-d datapoint taken from $\ln(P)$ and $\ln(\dot{P})$. The errors in $\ln(P)$ and $\ln(\dot{P})$ constitute the diagonal elements of their respective covariance matrices, with non-diagonal elements kept at zero, since we assume that the errors between the different pulsars are uncorrelated. These covariance matrices are vertically stacked and the resulting matrix is provided as input to the XDGMM algorithm. After running XDGMM, one can obtain the weights, means, and covariances for the specified number of clusters.

The number of Gaussian components used to fit this data is very important. We must ensure that the models do not underfit or overfit the data. Similar to most mixture models, XDGMM by itself does not determine the optimum number of clusters, and these are usually provided as inputs to the algorithm. In Lee et al. (2012), the optimum number of clusters were determined using a 2-D Kolmogorov-Smirnov (K-S) test. However, concerns about the validity of the 2-D K-S test have been raised in literature (Babu & Feigelson 2006)². Here, we treat the determination of optimum number of clusters as a model selection problem, and choose an information theory based metric, similar to our past work on GMM-based classification of GRBs and exoplanets (Kulkarni & Desai 2017, 2018).

3.3. Bayesian Information Criterion

² <https://asaip.psu.edu/articles/beware-the-kolmogorov-smirnov-test/>

The Bayesian Information Criterion (Schwarz 1978; Liddle 2007) score is an approximation to Bayesian evidence. BIC compensates for additional free parameters, and is widely used in astrophysics and cosmology for model comparison. The equation for BIC can be written as:

$$BIC = -2 \ln(\hat{L}) + k \ln(n), \quad (5)$$

where \hat{L} is the maximum likelihood of a given model, n is the size of the data set, and k is the total number of free parameters to be used to fit the model. BIC penalizes for additional number of free parameters, and hence aids in rejecting models which overfit the data. While comparing two models, the one with the lower BIC score is chosen as the optimum one.

For our analysis, we apply XDGMM with different number of clusters as inputs. For each of these choices, we compute the BIC score. These BIC scores as a function of the number of clusters used for classifying the pulsar data are plotted in Fig. 2. We find a minimum value of BIC for six clusters. Therefore, the optimum number of Gaussian clusters needed to fit the pulsar P - \dot{P} data including their errors is equal to six. This agrees with the analysis in Lee et al. (2012) and Ay et al. (2020), who also found six clusters using GMM and Dirichlet-GMM, respectively.

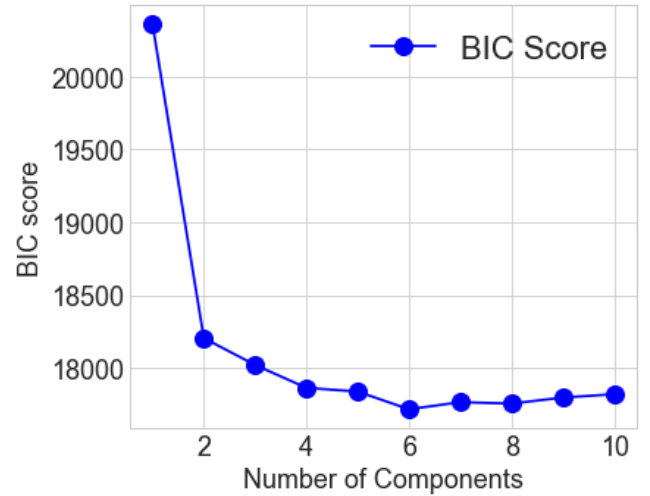


FIG. 2.— BIC Scores for the different number of Gaussian clusters used to fit the P and \dot{P} data.

3.4. Results

The resulting weights, mean and covariances of the six different Gaussian clusters, which can be used to classify the pulsar population in the P - \dot{P} logarithmic plane are tabulated in Table 1. The weights for each of the clusters agree with those obtained in Lee et al. (2012). However, the means and covariances show a slight deviation. Yet, the clusters are mostly at the same location as in Lee et al. (2012). Only one cluster has a mean with a positive value for $\ln(P)$, and only one covariance matrix has negative non-diagonal values. These observations are in accord with the corresponding means and covariances obtained in (Lee et al. 2012).

The means and covariances of the Gaussian clusters are used to plot 95% confidence interval (c.i.) ellipses

in the P - \dot{P} plane. The corresponding plots obtained by superimposing these confidence ellipses in the P - \dot{P} diagram are shown in Fig. 3. The two Gaussian clusters corresponding to the millisecond pulsars (MSPs) are independent of the clusters with high values for the period and larger magnetic fields. These two clusters constitute the pulsars, which belong to different binary star systems. The remaining four Gaussian clusters correspond to the normal pulsar population.

TABLE 1

THE GAUSSIAN CLUSTER PARAMETERS OBTAINED AFTER APPLYING XDGMM TO THE NATURAL LOG OF PULSAR P AND \dot{P} VALUES. $w_A, w_B \dots w_F$ DENOTE THE WEIGHTS OF THE GAUSSIAN CLUSTERS A,B ... F RESPECTIVELY; $\mu_A, \mu_B \dots \mu_F$ DENOTE THE CENTRAL VECTORS OF THE GAUSSIAN CLUSTERS A,B ... F, WHERE $\mu \equiv (\ln(P), \ln(\dot{P}))$; AND $\Sigma_A, \Sigma_B \dots \Sigma_F$ ARE THE COVARIANCE MATRICES.

Name	Value
w_A	0.0778
w_B	0.0474
w_C	0.2680
w_D	0.3952
w_E	0.1950
w_F	0.0166
μ_A	(-5.6162 -46.0092)
μ_B	(-3.9151 -43.0917)
μ_C	(-0.3868 -36.0364)
μ_D	(-0.5114 -33.6152)
μ_E	(-0.8092 -31.4473)
μ_F	(1.7131 -27.8876)
Σ_A	$\begin{bmatrix} 0.1466 & 0.068 \\ 0.068 & 0.9232 \end{bmatrix}$
Σ_B	$\begin{bmatrix} 1.3048 & 0.7306 \\ 0.7306 & 2.6998 \end{bmatrix}$
Σ_C	$\begin{bmatrix} 0.5583 & 0.8723 \\ 0.8723 & 3.6293 \end{bmatrix}$
Σ_D	$\begin{bmatrix} 0.5180 & 0.1212 \\ 0.1212 & 1.4940 \end{bmatrix}$
Σ_E	$\begin{bmatrix} 1.4273 & -0.2082 \\ -0.2082 & 2.6910 \end{bmatrix}$
Σ_F	$\begin{bmatrix} 0.2294 & 0.0647 \\ 0.0647 & 10.2614 \end{bmatrix}$

From the pulsar P and \dot{P} , one can estimate a characteristic age (τ_c) and the characteristic surface magnetic field (B_s) after making certain assumptions (Lorimer & Kramer 2012; Ay et al. 2020):

$$\tau_c = \frac{P}{2\dot{P}} \quad (6)$$

$$B_s = \left(\frac{3c^3 I}{8\pi^2 R^6} \right)^{\frac{1}{2}} \sqrt{P\dot{P}} \quad (7)$$

where I is the moment of inertia and R is the radius of the neutron stars. As in Ay et al. (2020), we assumed $I =$

10^{45} g cm^2 and $R = 10^6 \text{ cm}$. Therefore Eq. 7 simplifies to, $B_s = 3.2 \times 10^{19} \sqrt{P\dot{P}} \text{ G}$.

From these equations, we then proceed to calculate the characteristic age and surface magnetic field for each of the cluster populations using the mean (P and \dot{P}). The values of τ_c and B_s are tabulated in Table 2. These values are mostly in agreement with those in Table 5. of Ay et al. (2020).

3.5. Robustness of XDGMM

Igoshev & Popov (2013) have pointed out that the data classification using GMM does not produce stable results. They showed that exclusion of magnetars and thermally emitting neutron stars results in different clusters than the ones obtained in Lee et al. (2012). They also found that upon randomly removing 10% of the data points, the positions of the resulting clusters changes significantly. Hence, they concluded that GMM is oversensitive to small changes in the data, and consequently cannot be used for identifying evolutionary related groups in the pulsar distribution.

To check if our XDGMM-based classification runs into similar problems, we followed the same procedure as in Igoshev & Popov (2013). We carried out numerical experiments, by randomly removing 10% of the 2289 data points in each iteration, and then applied XDGMM for different number of Gaussian clusters. After repeating this procedure 30 times, we find that the positions of the clusters (after assuming the dataset contains six clusters) are similar to the ones obtained in Fig. 3, for most (77%) of the executions. There are only minor variations in the sizes, whereas the shapes vary slightly, and mostly only for the cluster on the extreme top right (marked F in Fig. 3). There were also few instances (23%), where a single cluster could encapsulate the millisecond pulsar population and five clusters for the rest of the data. However, the frequency of obtaining this result is quite low (23%).

The BIC scores for different number of Gaussian clusters for the reduced data set show a similar trend as in Fig. 2. The minimum value of BIC for 6 Gaussian clusters is obtained for 90% of our numerical experiments. Therefore, we conclude that our implementation of XDGMM is not sensitive to small changes in the dataset.

4. CONCLUSIONS

Two recent works in the past decade have classified the radio pulsar population along with other ancillary neutron star datasets, using unsupervised clustering techniques, such as GMM and Dirichlet mixture model (Lee et al. 2012; Ay et al. 2020). We carry out a similar exercise using XDGMM, which is an extension of GMM where errors in the observed variables are incorporated. Similar to the previous works, we carried out the classification using the logarithm of the period and period derivative. The optimum number of cluster was chosen using the BIC criterion from information theory.

When we apply this method to the latest catalog of radio pulsars, which we obtained from the online ATNF catalog, we find that the optimum number of clusters which can describe the radio pulsar population is equal to six. Two of these describe the millisecond pulsar pop-

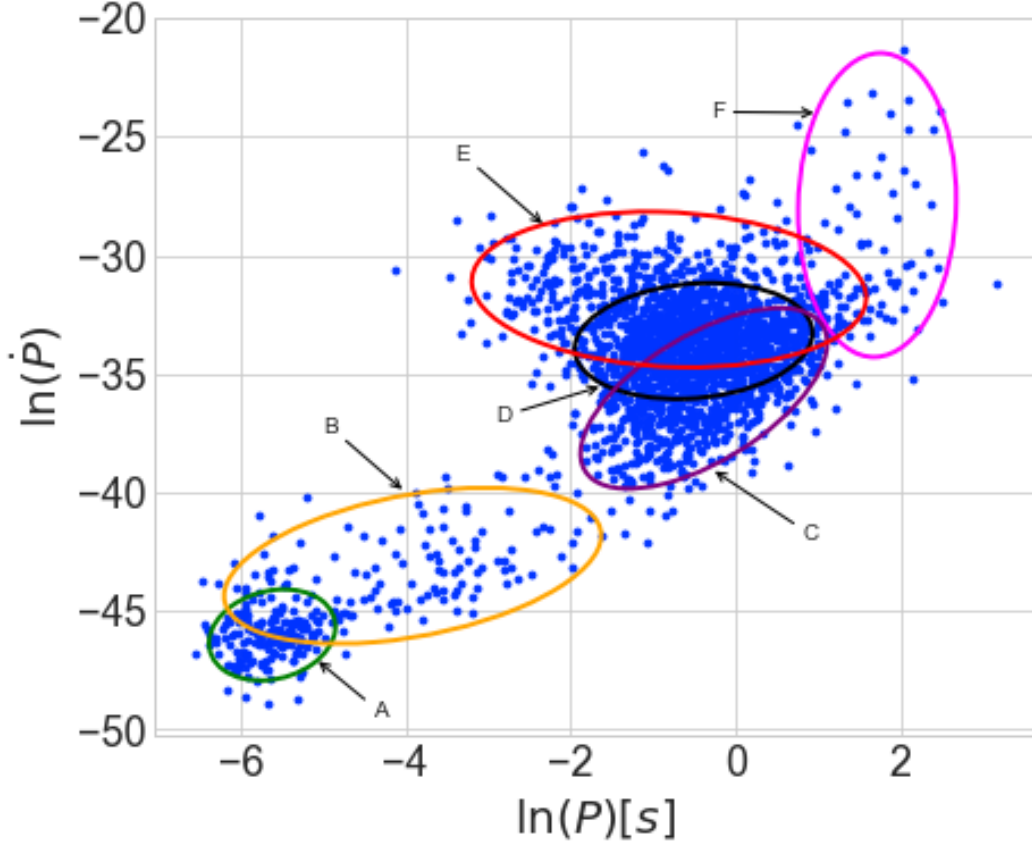


FIG. 3.— Pulsar P - \dot{P} diagram with Gaussian clusters, obtained after applying XDGMM. The ellipses denote the 95% c.i. contours for the six Gaussian clusters obtained from XDGMM. Clusters A and B describe the millisecond pulsars, whereas the remaining clusters encapsulate the rest of the radio pulsar population. More details about their properties can be found in Table 1 and Table 2.

TABLE 2
CHARACTERISTIC AGE AND DIPOLE MAGNETIC FIELD STRENGTH OF THE SIX GAUSSIAN CLUSTERS OBTAINED FROM EQ. 6 AND 7.

Name	Value (P (sec), \dot{P})	Characteristic Age (Yr)	Magnetic Field (Gauss)
μ_A	(0.0036 1.04×10^{-20})	5.52×10^9	1.97×10^8
μ_B	(0.019 1.9298×10^{-19})	1.63×10^9	1.98×10^9
μ_C	(0.68 2.23×10^{-16})	4.81×10^7	3.94×10^{11}
μ_D	(0.59 2.5×10^{-15})	3.77×10^6	1.24×10^{12}
μ_E	(0.44 2.20×10^{-14})	3.2×10^5	3.16×10^{12}
μ_F	(5.54 7.73×10^{-13})	1.13×10^5	6.62×10^{13}

ulation, whereas the remaining radio pulsar population can be grouped into four clusters. The 95% confidence level ellipses showing the full dataset centered on these clusters can be found in Fig. 3. The mean values and covariances of each of these clusters can be found in Table 1, and the characteristic ages and magnetic fields in

Table 2. These results are in accord with the previous works.

To promote transparency in data analysis, we have made available our codes and the data used for this analysis, which can be found at <https://github.com/taruntejreddych/XDGMM-for-Pulsar-classification>

REFERENCES

- Acero F., et al., 2015, *ApJS*, **218**, 23
 Ay F., Ince G., Kamaşak M. E., Ekşi K. Y., 2020, *MNRAS*, **493**, 713
 Babu G. J., Feigelson E. D., 2006, in Gabriel C., Arviset C., Ponz D., Enrique S., eds, *Astronomical Society of the Pacific Conference Series Vol. 351, Astronomical Data Analysis Software and Systems XV*. p. 127

- Ball N. M., Brunner R. J., 2010, *International Journal of Modern Physics D*, **19**, 1049
- Bhattacharya D., van den Heuvel E. P. J., 1991, *Phys. Rep.*, **203**, 1
- Blandford R. D., 1992, *Philosophical Transactions of the Royal Society of London Series A*, **341**, 177
- Bovy J., Hogg D. W., Roweis S. T., 2011, *Annals of Applied Statistics*, **5**, 1657
- Cordes J. M., Chatterjee S., 2019, *ARA&A*, **57**, 417
- Coronado-Blázquez J., Sánchez-Conde M. A., Di Mauro M., Aguirre-Santaella A., Ciucă I., Domínguez A., Kawata D., Mirabal N., 2019, *JCAP*, **2019**, 045
- De Luca A., 2017, in *Journal of Physics Conference Series*. p. 012006 ([arXiv:1711.07210](#)), [doi:10.1088/1742-6596/932/1/012006](#)
- Desai S., Kahya E. O., 2016, *Modern Physics Letters A*, **31**, 1650083
- Enoto T., Kisaka S., Shibata S., 2019, *Reports on Progress in Physics*, **82**, 106901
- Fluke C. J., Jacobs C., 2020, *WIREs Data Mining and Knowledge Discovery*, **10**, e1349
- Fraix-Burnet D., Thuillard M., Chattopadhyay A. K., 2015, *Frontiers in Astronomy and Space Sciences*, **2**, 3
- Glushak A. P., 2020, *Astronomy Reports*, **64**, 602
- Harding A. K., 2013, *Frontiers of Physics*, **8**, 679
- Hewish A., Bell S. J., Pilkington J. D. H., Scott P. F., Collins R. A., 1968, *Nature*, **217**, 709
- Holoien T. W. S., Marshall P. J., Wechsler R. H., 2017, *AJ*, **153**, 249
- Igoshev A. P., Popov S. B., 2013, *MNRAS*, **434**, 2229
- Ivezić Ž., Connolly A., Vanderplas J., Gray A., 2014, *Statistics, Data Mining and Machine Learning in Astronomy*. Princeton University Press
- Kaspi V. M., 2010, *Proceedings of the National Academy of Science*, **107**, 7147
- Kaspi V. M., Kramer M., 2016, arXiv e-prints, p. [arXiv:1602.07738](#)
- Keitel D., 2019, *MNRAS*, **485**, 1665
- Konar S., 2017, *Journal of Astrophysics and Astronomy*, **38**, 47
- Koposov S. E., Belokurov V., Evans N. W., 2013, *ApJ*, **766**, 79
- Kramer M., Stappers B., 2015, in *Advancing Astrophysics with the Square Kilometre Array (AASKA14)*. p. 36 ([arXiv:1507.04423](#))
- Kuhn M. A., Feigelson E. D., 2017, arXiv e-prints, p. [arXiv:1711.11101](#)
- Kulkarni S., Desai S., 2017, *Ap&SS*, **362**, 70
- Kulkarni S., Desai S., 2018, *The Open Journal of Astrophysics*, **1**, 4
- Lee K. J., Guillemot L., Yue Y. L., Kramer M., Champion D. J., 2012, *MNRAS*, **424**, 2832
- Liddle A. R., 2007, *MNRAS*, **377**, L74
- Lorimer D. R., Kramer M., 2012, *Handbook of Pulsar Astronomy*
- Manchester R. N., 2017, in *Journal of Physics Conference Series*. p. 012001 ([arXiv:1801.04323](#)), [doi:10.1088/1742-6596/932/1/012001](#)
- Manchester R. N., Hobbs G. B., Teoh A., Hobbs M., 2005, *AJ*, **129**, 1993
- Nolan P. L., et al., 2012, *ApJS*, **199**, 31
- Roche A., 2011, arXiv e-prints, p. [arXiv:1105.1476](#)
- Safi-Harb S., 2017, in *Journal of Physics Conference Series*. p. 012005 ([arXiv:1712.06040](#)), [doi:10.1088/1742-6596/932/1/012005](#)
- Schwarz G., 1978, *Annals of Statistics*, **6**, 461
- Tarnopolski M., 2019, *ApJ*, **887**, 97
- Vivekanand M., Narayan R., 1981, *Journal of Astrophysics and Astronomy*, **2**, 315
- Vranešević N., Melrose D. B., 2011, *MNRAS*, **410**, 2363
- Woods P. M., Thompson C., 2006, *Soft gamma repeaters and anomalous X-ray pulsars: magnetar candidates*. pp 547–586